Available online at www.sciencedirect.com
SCIENCE DIRECT®
International Journal of Thermal Sciences 43 (2004) 797–808
International Journal of Thermal Sciences
www.elsevier.com/locate/ijts

Numerical investigation of flow reversal and instability in mixed laminar vertical tube flow

Cong Tam Nguyen [a,*], Sidi El Bécaye Maïga [a], Mathieu Landry [a], Nicolas Galanis [b], Gilles Roy [a]

[a] *Faculty of Engineering, Université de Moncton, Moncton, NB, E1A 3E9 Canada*
[b] *Department of Mechanical Engineering, Faculty of Engineering, Université de Sherbrooke, Sherbrooke, PQ, J1K 2R1 Canada*

Received 20 August 2003; received in revised form 19 December 2003; accepted 24 February 2004

Available online 10 June 2004

Abstract

The problem of the transient laminar mixed convection flow of air in a vertical tube under buoyancy effect and high wall heat flux condition has been numerically investigated by using a full 3D-transient-model and Boussinesq's assumptions. The tube is submitted to a uniform but time-dependent wall heat flux. Results have clearly shown that the flow reversal was first initiated near the tube exit section, on the tube wall and at the level $Gr = 3 \times 10^5$ for opposed-buoyancy case, and on the tube centerline and at the level of Grashof number around 10^6 for assisted-buoyancy one. With further increase in time of the wall heat flux, such reversed flow region has considerably increased in size and intensity and it clearly spreads into the upstream region. The presence of such recirculation cells has drastically perturbed the flow and the thermal field as well as the heat transfer. Although the flow structure appears to conserve its axisymmetrical characters even for cases with very high Grashof numbers, results from this study have shown that the flow seems to remain stable and unique up to the level $Gr = 5 \times 10^5$ and 10^6, respectively, for opposed and assisted buoyancy cases. Beyond these critical Grashof numbers, an extremely slow and rather difficult and tedious convergence behaviors have been experienced, which are believed to be due to a possible flow transition.

Keywords: Heat transfer; Fluid flow; Laminar flow; Reversal flow; Mixed convection; Transient behaviors; Opposed-buoyancy; Assisted-buoyancy; Instability; Transition; Numerical simulation

1. Introduction

Because of its wide applications in engineering, the laminar mixed convection flow has received a rather particular attention from researchers in the past decades. A partial review of relevant works in the domain may be found in [1,2]. A following brief review is emphasised on the flow reversal phenomenon and the flow instability in a vertical tube. For such configuration, the pioneers works by Hanratty and colleagues in the early sixties [3,4] have clearly shown that the non-isothermal flow appears to be highly unstable and may undergo its transition from a steady laminar state to an unstable one at rather low Reynolds number. The unstable flow structure, which was not turbulent, has shown, in fact, the 'new equilibrium' state that consisted of large scale, regular and periodic fluid motions. These authors have also found that for heated upward flow (assisted-buoyancy), instabilities may occur when the velocity profiles develop points of inflexion; while for heated downward flow (opposed-buoyancy), the instability seems to be associated with the flow separation from the tube wall. Regarding the flow reversal in particular, one can mention very interesting results and experimental observations performed by Lavine and colleagues [5,6] for the case of opposed-buoyancy flow in heated inclined tubes. They have found that the flow reversal may trigger early transition to the turbulence. Their temperature measurements have clearly shown periodic behaviours in the flow reversal region for low tube inclination and moderate to high Reynolds and Grashof numbers. Such periodic behaviours appear to be caused by an intermittent breakdown of the reversed flow region. Wang and colleagues [7] have investigated the problem of mixed convection with flow reversal in the thermal entrance region of horizontal and vertical pipes at low Péclet number. For a vertical tube flow, they have found that the flow reversal occurs

* Corresponding author. Fax: +1 (506) 858-4082.
E-mail address: nguyenc@umoncton.ca (C.T. Nguyen).

1290-0729/$ – see front matter
doi:10.1016/j.ijthermalsci.2004.02.020

Nomenclature

C_p	specific heat of the fluid	$J{\cdot}kg^{-1}{\cdot}K^{-1}$
D	tube diameter	m
Gr	Grashof number, Eq. (9)	
Nu_Z	local Nusselt number, $= h_Z D/k_0$	
Pr	Prandtl number, Eq. (9)	
R	radial coordinate	m
Re	Reynolds number, Eq. (9)	
R_0	tube radius	m
T	fluid temperature	K
T_{amb}	ambient fluid temperature	K
T_0	inlet fluid temperature	K
V_0	average axial velocity at tube inlet	$m{\cdot}s^{-1}$
V_R	radial velocity component	$m{\cdot}s^{-1}$
V_θ	tangential velocity component	$m{\cdot}s^{-1}$
V_Z	axial velocity component	$m{\cdot}s^{-1}$
Z	axial coordinate	m
g	gravitational acceleration	$m{\cdot}s^{-2}$
h_Z	local heat transfer coefficient	$W{\cdot}m^{-2}{\cdot}K^{-1}$
k	thermal conductivity of the fluid	$W{\cdot}m^{-1}{\cdot}K^{-1}$
p	pressure	Pa
p_{amb}	ambient fluid pressure	Pa
q''_W	wall heat flux	$W{\cdot}m^{-2}$

Greek letters

Φ	dependent variable	
β	coefficient of thermal expansion	K^{-1}
θ	circumferential coordinate	rad
μ	fluid dynamic viscosity	$kg{\cdot}m^{-1}{\cdot}s^{-1}$
ρ	fluid density	$kg{\cdot}m^{-3}$
τ	time	s

Subscripts

amb	refers to the ambient conditions in the surrounding space
W	refers to tube wall
0	refers to the reference condition

at the pipe center for the heating case and near the tube wall for the cooling case, both at relatively high $|Gr/Re|$ ratio. Different regimes of reversed flow have been identified for both cases in a $Pe - |Gr/Re|$ coordinate map. In their recent works [8,9], the authors have numerically investigated the problem of laminar upward flow in vertical tube with a uniformly heated zone preceded and followed by adiabatic zones, using a fully-elliptic model and considering wide range of heating lengths, Reynolds and Richardson numbers. Results have clearly shown that, depending upon the combination of these parameters, it may exist five different flow regimes with or without reversals. The conditions leading to the flow reversal as well as the significance of the upstream axial diffusion of heat and momentum have also been established and the results have been mapped on the Péclet–Richardson numbers plane for different lengths of the heated zone. Most recently, Behzadmehr and colleagues [10] have investigated similar problem of laminar mixed convection of upward air flow in vertical tube, by judiciously employing a low-Reynolds-number turbulent model to performing calculations for both the laminar and turbulent flow regimes. The results have shown that under buoyancy effect, the flow transition to turbulence may occur at relatively low Reynolds number, and the existence of two different critical Grashof numbers for which transition occurs has clearly been established. At the first critical Grashof number, the flow changes from the laminar regime to the turbulent one, and at the second one with higher wall heat flux, another transition occurs and the flow goes back to its original laminar regime. The numerical results have also shown two different reversal patterns: the first one is located on the tube centreline; while the second one is observed between the axis and the wall.

In real industrial applications, however, a transient laminar flow may occur during normal operation or, most often, due to accidents. Unfortunately, such flow seems not to receive much attention in the past [1]. With regard to the problem of an unsteady laminar mixed convection flow subject to time-dependent boundary conditions at the tube inlet, references [11–13] are relevant. In a recent work [14], Mai and colleagues have investigated the problem of a transient vertical laminar flow submitted to a step change of the inlet flow rate. Results have shown that both the buoyancy and the external convective heat transfer condition have an important effect on the flow and also on the local Nusselt number. The problem of laminar mixed flow subject to a step change of fluid inlet temperature has been investigated as well [15]. For the heating case, the reversed flow appears below the wave instability; with an increase of the Richardson number, the unsteady vortex becomes more important at the interface between the boundary layer and the core region. For the cooling cases, results have shown that the effect of the wall-to-fluid heat capacity ratio becomes more significant. The formation of the unsteady vortex appears on top of the wave instability.

It is important to note that, unfortunately, the influence of the flow reversal on the onset of the instabilities has not been very well understood to date [1]. The first theoretical study of the stability of mixed laminar convection flow was likely due to Yao [16,17] who has performed a linear stability analysis for water flow in a heated vertical tube. He has found that the fully-developed non-isothermal flow appears highly unstable, and the 'bifurcated new equilibrium' flow state is likely to be a double helices structure. Such unstable flow structure seems to be susceptible to delaying its transition to turbulence. Yao and Rogers [18] have also con-

tributed important work on the thermal instability mechanism in a vertical annulus. In a most recent linear stability analysis, Su and Chung [19] have provided very interesting information regarding the instability mechanism as well as the effects of the Prandtl number. The results presented have suggested that the mixed laminar convection flow in a vertical tube may become unstable at low Reynolds number and Rayleigh numbers irrespectively of the fluid Prandtl number. For water in particular, their predicted values for the critical Rayleigh number agree very well with the corresponding experimental data by Scheele and Hanratty [4] for both assisted and opposed buoyancy cases. Su and Chung have also found that the Prandtl number profoundly affects the stability of an assisted-buoyancy flow and changes its instability mechanism as well. For Prandtl less than 0.3, the thermal-shear instability is dominant; while for $Pr > 0.3$, the assisted-thermal-buoyant instability becomes responsible. On the other hand, for the opposed-buoyancy case, the influence of the Prandtl number seems to be less significant, which is attributed, according to these authors, to the fact that such flow is itself unstably stratified.

The above stability analyses, all based on the linear perturbations method, have shed interesting insight into the rather complex nature of the instabilities that may occur in a fully-developed laminar mixed convection flow. Since these studies assume infinitesimal perturbations, i.e., quasi-steady flow regimes may be approximated, it becomes highly questionable whether the results obtained from such studies can be applied for predicting the flow behaviours under real operational conditions for which, transient and large disturbances may often be encountered.

In the present work, we have numerically studied the structure of the flow and the thermal field for a simultaneously developing laminar mixed convection flow and its transient behaviours under strong and time-dependent heating condition i.e., high Grashof number. The results are presented and discussed with emphasis on the occurrence of the flow reversal phenomenon as well as its effects on the heat transfer rate.

2. Mathematical modeling and numerical method

The problem consists of the simultaneously developing mixed convection flow of air inside a vertical tube of diameter $D = 10$ mm and length $L = 200$ mm, which is submitted to a uniform but time-dependent wall heat flux, Fig. 1. The flow is assumed transient, laminar and *a priori* three-dimensional, that is to say no assumption regarding the flow symmetry is invoked. The fluid is considered viscous and incompressible with constant physical properties except for its density that appears in the buoyancy terms (the Boussinesq's assumptions). Both the compression work and the viscous dissipation are considered negligible. Under such assumptions, the corresponding governing equations,

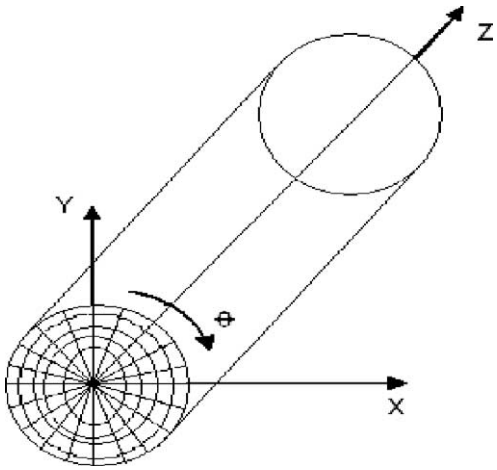

Fig. 1. Geometrical configuration of the problem studied.

as derived from the principle of the conservation of mass, momentum and energy, are as follows [20]:

$$\nabla \cdot (\rho_0 \boldsymbol{V}) = 0 \tag{1}$$

$$\partial(\rho_0 V_R)/\partial\tau + \nabla \cdot (\rho_0 \boldsymbol{V} V_R) = -\partial p/\partial R + \nabla \cdot (\mu_0 \nabla V_R) + S_R \tag{2}$$

$$\partial(\rho_0 V_\theta)/\partial\tau + \nabla \cdot (\rho_0 \boldsymbol{V} V_\theta) = -(1/R)\partial p/\partial\theta + \nabla \cdot (\mu_0 \nabla V_\theta) + S_\theta \tag{3}$$

$$\partial(\rho_0 V_Z)/\partial\tau + \nabla \cdot (\rho_0 \boldsymbol{V} V_Z) = -\partial p/\partial Z + \nabla \cdot (\mu_0 \nabla V_Z) + \rho_0 g \beta_0 (T - T_0) \tag{4}$$

$$\partial(\rho_0 C_{p0} T)/\partial\tau + \nabla \cdot (\rho_0 \boldsymbol{V} C_p T) = \nabla \cdot (k_0 \nabla T) \tag{5}$$

where $\boldsymbol{V} = (V_r, V_\theta, V_Z)$ is the fluid velocity vector; τ and p are the time and the pressure; ρ, μ, k and C_p are, respectively, the fluid density, dynamic viscosity, thermal conductivity and specific heat; the subscript 0 refers to the reference condition corresponding to the fluid inlet temperature T_0. The terms S_R and S_θ are velocities-related stress terms that result from the choice of the cylindrical coordinate system; they are given as follows:

$$S_R = \rho_0 V_\theta^2/R - \mu_0\left[\left(V_R/R^2\right) + \left(2/R^2\right)(\partial V_\theta/\partial\theta)\right] \tag{6}$$

$$S_\theta = -\rho_0 V_R V_\theta/R + \mu_0\left[\left(2/R^2\right)\left(\partial V_R/\partial\theta\right) - \left(V_\theta/R^2\right)\right] \tag{7}$$

2.1. Boundary and initial conditions

The governing equations (1)–(5) are non-linear and strongly coupled each other. They are subject to the following boundary and initial conditions:

2.1.1. Boundary conditions

– *At the tube inlet*, the fluid has uniform profiles of axial velocity V_0 and temperature T_0:

$$Z = 0; \quad R = 0,\ D/2; \quad \theta = 0, 2\pi$$
$$V_R = V_\theta = 0, \quad V_Z = V_0, \quad T = T_0 \tag{8a}$$

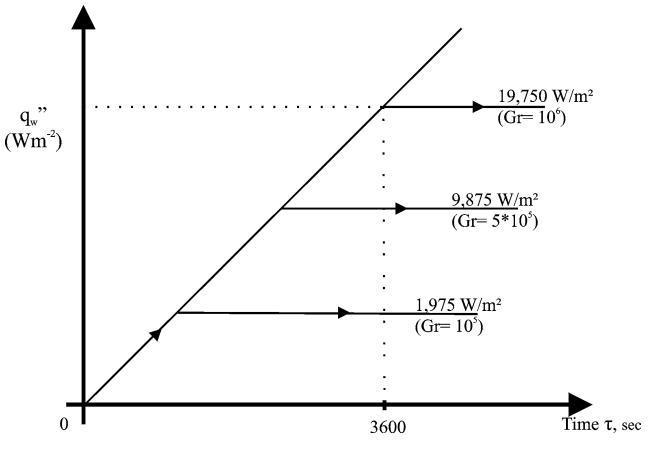

Fig. 2. Time-variation of heat flux q''_W as imposed on tube wall.

– *At the tube wall*, the usual non-slip conditions prevail. Also, a uniform but time-dependent heat flux, which varies as a linearly function of time (Fig. 2), is prescribed:

$$Z = 0, L; \quad R = D/2; \quad \theta = 0, 2\pi$$
$$V_R = V_\theta = V_Z = 0, \quad q''_W = f(\tau) \tag{8b}$$

– *At the tube exit section*, the so-called 'pressure outlet' conditions with a specified known pressure p_{amb} and ambient temperature T_{amb} are prescribed. These parameters, for the problem under consideration, correspond in fact to the ambient conditions that prevail in the outer space adjacent to the tube outlet section. They have been assigned, as values, atmospheric pressure and 300 K, respectively for p_{amb} and T_{amb} (that is, if there is any reversal flow through the tube exit section, the intake fluid that comes from the outer space will have 300 K as temperature; further details regarding such boundary condition and its treatment may be found in [22]).

2.1.2. Initial conditions

We assume that at the beginning of the heating process i.e., at time $\tau = 0$, the fluid has uniform temperature T_0 throughout the domain and its velocity field corresponds, in fact, to that of the classical case of developing laminar 'pure forced' flow (i.e., with $Gr = 0$) at the same Reynolds number considered.

2.1.3. Dimensionless parameters

One can determine that the problem under consideration may be characterized by a set of three dimensionless parameters, namely the Reynolds number, the Prandtl number and the Grashof number. Their definition is given as follows:

$$Re = V_0 D\rho_0/\mu_0; \qquad Pr = C_{p0}\mu_0/k_0$$
$$Gr = \rho_0^2 g\beta_0 q''_W D^4/\left(\mu_0^2 k_0\right) \tag{9}$$

2.2. Numerical method and code validation

The system of the governing equations (1)–(5), which is constituted of non-linear and strongly coupled PDE, has been successfully solved by using the numerical method that is essentially based on the well known 'control-volume approach', in which, the spatial integration is performed for each of the governing equations over finite-control volumes [21,22]. The power-law scheme has been employed throughout to compute the heat and momentum fluxes, while a fully implicit second-order temporal scheme has been adopted for the treatment of the transient terms of the governing equations [22]. On the other hand, the standard SIMPLE-procedure has been employed in order to handle the pressure-velocity coupling. The resulting 'discretization equations' have been solved in a sequential manner, i.e., one at a time, using the combination of the efficient multiple-and-alternate-sweeping technique, the 'line-by-line' technique and the standard TDMA ('Three-Diagonal Matrix Algorithm'). Complete information regarding the numerical method are well documented elsewhere [21,22]. In order to ensure the accuracy of the results, and more importantly, their independence with respect to the number of nodes used in the discretization process, several grids were thoroughly tested and the $25 \times 32 \times 90$ non-uniform grid has been found to be appropriate for the problem under study. Such adopted grid has respectively 25, 32 and 90 nodes in the radial, tangential (covering 0–360°) and axial directions with highly packed grid points near the tube wall, in the entrance region as well as in the exit region. A time step varying from 0.l–2.5 s has been found sufficient and adequate in order to detect and follow any change of the flow field during its heating process. As general numerical procedure, we started from the velocities and thermal fields corresponding to an isothermal 'pure forced' convection case (i.e., $Gr = 0$) and then proceeded, by increasing progressively (i.e., in time) the wall heat flux q''_W, to reaching another level of Gr. For some particular levels of interest, extended calculations have been pursued in time at the same value of q''_W that has been reached in order to allow sufficient time for the flow to develop. During all of such calculations, the flow and thermal field were constantly and carefully scrutinized in order to ascertain their structures as well as their nature, either stable or unstable, in particular for the opposed-buoyancy cases under high heat flux condition for which the occurrence of the flow reversal phenomenon may likely occur. As convergence indicator, we have essentially based on the residuals that result from the 'discretized form' of the governing equations (1)–(5). During the iterative calculation process, these residuals were constantly monitored and carefully scrutinized. For most of the simulations performed in this study, converged solutions have usually been achieved with residuals as low as 10^{-8} for all of the governing equations.

The computer model has been successfully validated by comparing the results as obtained for the development of the axial velocity component as well as that of the local

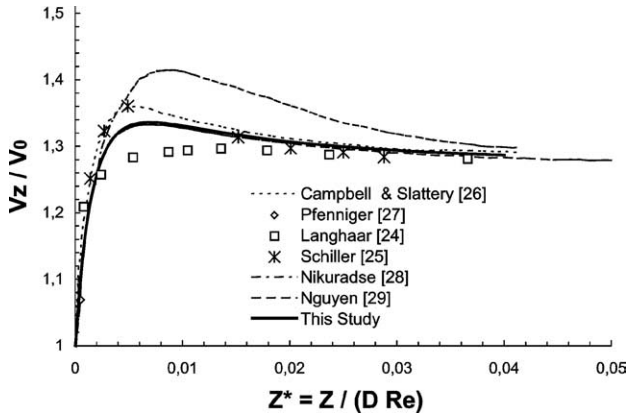

(a)

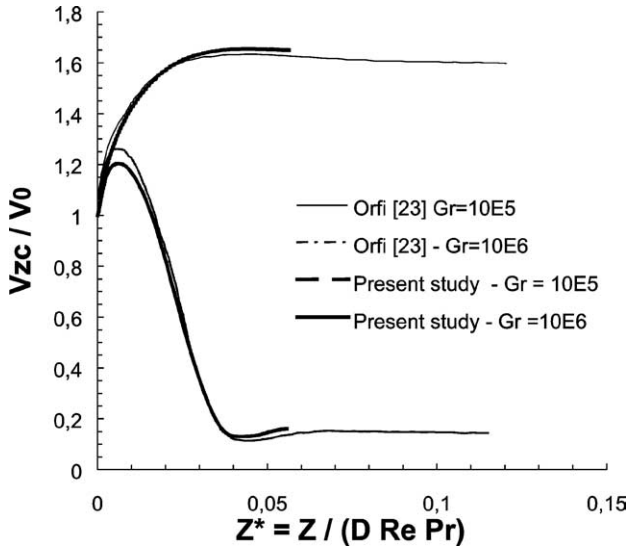

(b)

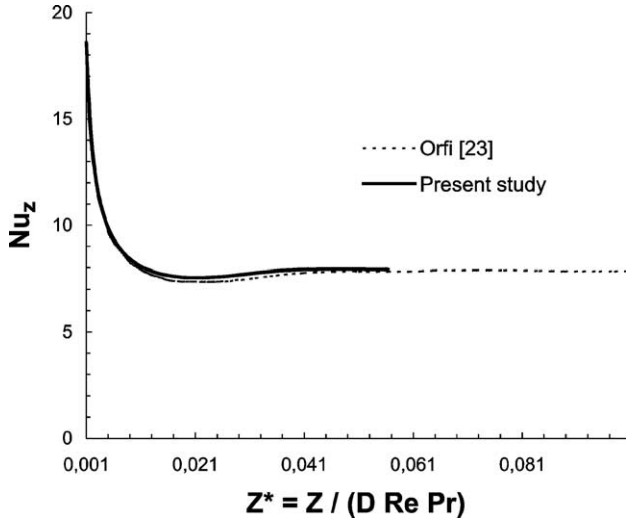

(c)

Fig. 3. Comparison with other analytical and numerical data for: (a) Axial development of V_Z at $R = 0.3D$ for laminar forced convection flow ($Gr = 0$); (b) Axial development of V_Z at $R = 0$ for mixed convection air flow ($Gr = 10^5$, 10^6); (c) Axial development of Nusselt number for mixed convection air flow ($Gr = 10^6$).

Nusselt number Nu_Z, to the corresponding analytical and numerical data available in the literature, for (i) the classic case of an isothermal developing laminar forced flow in a tube, Fig. 3(a), and (ii) the case of the steady, laminar mixed convection upward flow of air in a uniformly heated vertical tube [23], Fig. 3(b) and (c). As one can notice, the agreement between our results and others', in particular with Orfi's data [23] for cases under high Grashof number condition, may be qualified as very good. Therefore, we can conclude with confidence about the appropriateness of the mathematical model as well as the reliability of the chosen numerical method.

3. Results and discussion

In order to study the transient behaviors of the flow and the thermal field under the perturbations resulting from the imposition of time-dependent wall heat flux, extensive calculations were performed for air and the following fixed parameters: $T_0 = 300$ K, $Pr = 0.708$, $Re = 500$; the wall heat flux q''_W varies linearly with time with a constant slope of 5.486 $\mathrm{W{\cdot}m^{-2}{\cdot}s^{-1}}$, Fig. 2. For the results shown in the present paper, q''_W has varied from 0 to 19 750 $\mathrm{W{\cdot}m^{-2}}$ for downward heated flow (opposed-buoyancy) and from 0 to 34 560 $\mathrm{W{\cdot}m^{-2}}$ for upward heated flow (assisted-buoyancy) which correspond, respectively, to the ranges 0–10^6 and 0–1.75×10^6 of the Grashof number.

3.1. Transient evolution of axial velocity and temperature profiles

Figs. 4(a), (b) show the temporal development of the fluid axial velocity and temperature profiles as obtained for several heated downward (opposed-buoyancy) cases and a specific axial location $Z = 195$ mm near the exit section. These profiles correspond to different values of the Grashof number, i.e., to different times during the heating process (see again Fig. 2). It is important to mention that the profiles corresponding to the 'critical' cases $Gr = 7.5 \times 10^5$ and 10^6 are actually not converged results, in spite of relatively low residuals (details will be given later in Section 4). One can observe at first, Fig. 4(a), that the flow field seems to remain axisymmetrical even for cases with sufficiently high Grashof number as the ones considered in this study. Thus, for the case $Gr = 0$, i.e., at time $\tau = 0$, the flow field corresponds to the case of 'pure forced' flow without natural convection effect and hence, exhibits a perfect parabolic axial velocity profile (we note that for the case considered, the flow is not fully developed at the axial location $Z = 195$ mm). With further increase in time and, correspondingly, the wall heat flux q''_W, the opposing buoyancy effects near the tube wall become more pronounced that act again the main downward flow. Thus, one can observe that the fluid is clearly decelerated in the near wall region. At the particular level $Gr = 3 \times 10^5$, i.e., $q''_W = 5\,925$ $\mathrm{W{\cdot}m^{-2}}$, the radial

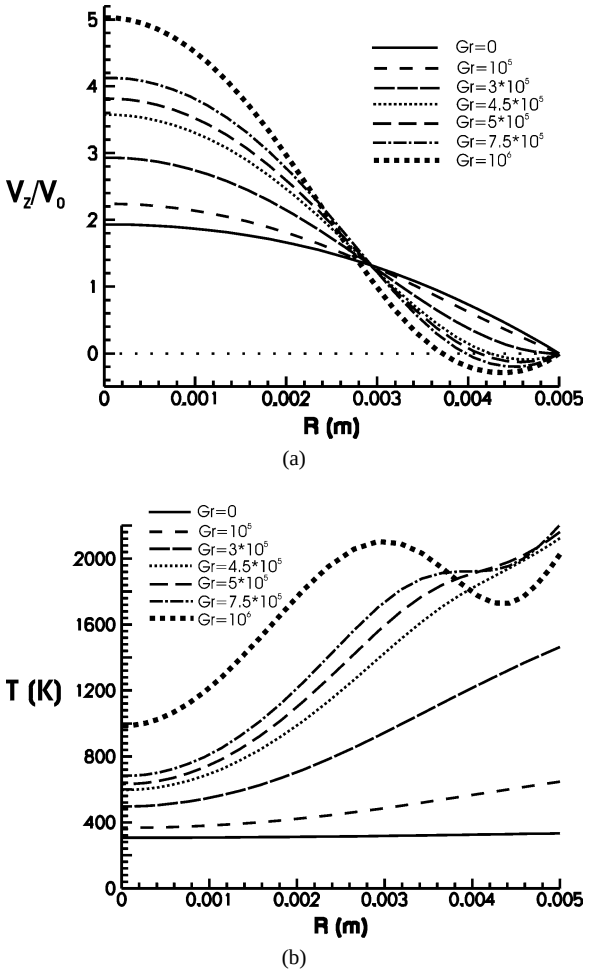

Fig. 4. Transient evolution of (a) axial velocity and (b) temperature profiles, for opposed-buoyancy case.

gradient of V_Z vanishes, in fact, on the tube wall indicating obviously that the flow reversal has just been initiated. Associated with such phenomenon, we can clearly observe a strong acceleration of fluid in the core region. With further increase of q''_W, negative axial velocities become more visible near the wall and the thickness of the reversed flow region also increases considerably; the fluid acceleration in the core region has become, consequently, more important. Thus for example, the velocity ratio V_Z/V_0 on the tube centreline has as values, 1.95, 2.22, 2.92, 3.58, 3.83 and 4.13, respectively, for $Gr = 0$, 10^5, 3×10^5, 4.5×10^5, 5×10^5 and 7.5×10^5; while for the extreme case $Gr = 10^6$, such ratio has reached a value as high as 5.03. On the other hand, it is observed that the thickness of the reversed flow region has almost doubled between the case $Gr = 4.5 \times 10^5$ and 10^6. Such rather striking effect due to the flow reversal on the fluid radial temperature profile can also be observed in Fig. 4(b) for the same axial location. Thus, one can see that for the case $Gr = 3 \times 10^5$ where the flow reversal was first detected and also for the case $Gr = 4.5 \times 10^5$ where a relatively 'mild' reversed flow has already set in, there is practically no perceptible effect on the temperature profile except for a strong heating effect in the near wall region, effect that obviously increases with an augmentation of q''_W However, for the cases $Gr = 5 \times 10^5$, 7.5×10^5 and 10^6, the presence of a reversed flow region has drastically distorted the temperature profile, especially in the near wall region where one can remark a clear change in the shape of fluid temperature profiles. Also, it is very interesting to see that, in the vicinity of the tube wall, say for $R/R_0 > 0.82$ approximately, fluid temperature profiles for the cases $Gr = 5 \times 10^5$ and 7.5×10^5 are very close each other. For the extreme case $Gr = 10^6$ in particular, the presence of a strong reversed flow near the wall has even produced more pronounced effects as we can see in a highly distorted fluid temperature profile, Fig. 4(b). Such profile exhibits a rather curious shape with two local minima, one observed on the centerline and the other one located in the near wall region, say at $R/R_0 \approx 0.88$. For that case, while the heating effect is clearly present in the core region, in the near wall region however, fluid temperatures are, surprisingly, much lower than those of cases $Gr = 4.5 \times 10^5$, 5×10^5 and 7.5×10^5. It is also observed that the radial temperature gradient has considerably increased on the tube wall, indicating obviously that heat transfer has become more important at this axial location. Such behaviors regarding the temperature profiles of the cases $Gr = 5 \times 10^5$, 7.5×10^5 and 10^6 are due, in fact, to the presence of a recirculation zone near the wall that has bring colder fluid from the outer space adjacent to the tube exit section into the upstream region, as we may see later on the corresponding streamlines.

Figs. 5(a), (b) show, for the case of upward heated flow (assisted-buoyancy) and several specific times of interest during the heating process, the corresponding axial velocity and temperature profiles as obtained for the same axial location considered earlier ($Z = 195$ mm). It should be noted that the results corresponding to the cases $Gr = 1.5 \times 10^6$ and 1.75×10^6 are actually not converged results. In fact, for these 'critical' cases, we were unable to obtain converged asymptotic solution that corresponds to a constant level of q''_W (more details and discussion will be given later in Section 4). One can observe that with the aiding buoyancy effect, the fluid axial velocity in the near wall region has appreciably augmented. Such effect clearly becomes more important for cases with sufficiently high Grashof numbers, and this to the detriment of fluid located in the core region where one can easily observe an important deceleration of fluid. Thus, for the values considered of the Grashof number, $Gr = 0$, 10^5, 5×10^5 and 10^6, the velocity ratio V_Z/V_0 on the tube centreline has respectively as values, 1.95, 1.65, 0.74 and 0.17. For the particular cases $Gr = 1.5 \times 10^6$ and 1.75×10^6, V_Z at $R = 0$ becomes strongly negative, with respectively $V_Z/V_0 \approx -0.88$ and -1.0, indicating obviously the presence of a well established reversed flow region on the tube centerline. From these results, one can expect that the flow reversal would be initiated for a Grashof number around 10^6. Such reversed flow becomes more pronounced and clearly increases in size with further

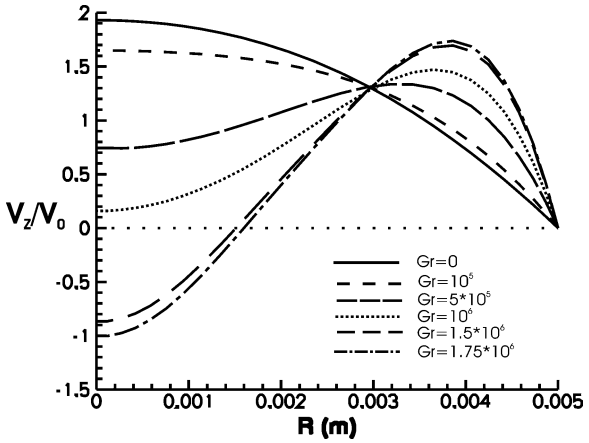

(a)

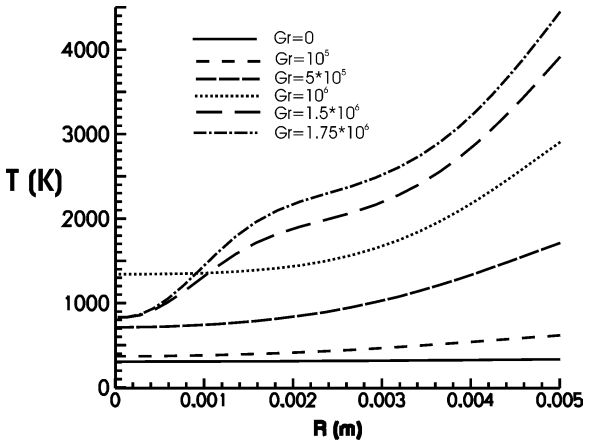

(b)

Fig. 5. Transient evolution of (a) axial velocity and (b) temperature profiles, for assisted-buoyancy case.

increase in time (and hence of q''_W). For example, at the axial position considered, it occupies a region extended from $R/R_0 = 0$ to nearly 0.3 and 0.32 for the cases $Gr = 1.5 \times 10^6$ and 1.75×10^6. As observed before for the opposed-buoyancy cases, results have shown that even for such high Grashof numbers, the flow field as obtained for the assisted-buoyancy cases also appears to conserve its axisymmetrical character. The effects due to the flow reversal on fluid temperature profiles may be scrutinized in Fig. 5(b) for the same axial location considered. Thus, it is observed that under the increase in time of the wall heat flux q''_W and aiding buoyancy, heating effect obviously becomes more pronounced in particular in the near wall region where the radial temperature gradient has considerably increased with the Grashof number. For the cases $Gr = 1.5 \times 10^6$ and 1.75×10^6 in particular, the presence of reversed flow in the core region has bring colder fluid from the outer space adjacent to the tube exit section into the upstream region, as shown in the next paragraph. As consequence, we can observe that fluid temperature on the tube centerline has, in fact, decreased from 1350 K to nearly 840 K for Gr increasing from 10^6 to 1.5×10^6; such temperature is almost identical for both cases $Gr = 1.5 \times 10^6$ and 1.75×10^6. On the other hand, the radial gradient of fluid temperature on the wall has considerably increased for cases $Gr = 1.5 \times 10^6$ and 1.75×10^6, which clearly indicates a more pronounced heat transfer rate at the wall at the axial location considered.

3.2. Transient evolution of the flow and thermal fields

The above striking effect due to the presence of the reversed flow region in the case of opposed-buoyancy flow may be better understood by scrutinizing the structure of the flow and thermal fields as obtained for different times that correspond to the following values of the Grashof number, $Gr = 4.5 \times 10^5$, 5×10^5, 7.5×10^5 and 10^6. Figs. 6(a)–(d) show isotherms and iso-contours of V_Z for these cases. It should be noted that the radial coordinate has been arbitrarily exploded in order to gain into fine details of the flow structure and thermal field; dotted lines show regions of negative V_Z while lines $V_Z = 0$ indicate the boundary of the reversed region. We note at first, that for the case $Gr = 3 \times 10^5$ (not shown) for which the flow reversal has just been initiated on the wall near the tube exit section (see again Fig. 4(a)), there is no perceptible change on both the flow and temperature field. They correspond almost to those of the 'pure-forced' convection case, except for the region immediate to the exit section where one can observe a mild acceleration of fluid in the core region; the velocity ratio V_Z/V_0 is slightly superior than 2. With further increase of q''_W in time, say for case $Gr = 4.5 \times 10^5$, Fig. 6(a), the reversed flow region now appears more visible near the wall; it is approximately extended from the axial position $Z = 0.1$ m up to the tube exit. Due to such recirculation cell, fluid acceleration inside the core region now becomes more important and is observed over a longer zone prior to the exit section. Also, it has created a tiny pocket of high fluid temperature on the tube wall near the exit; as consequence, we can observe that isotherms are curved therein. Such rather interesting effects become more important with further increase of q''_W. Thus, the reversed flow region increases considerably and is clearly spreading upstream; in fact, the fluid separation from the wall is approximately observed at the following axial locations $Z = 0.09$, 0.06 and 0.04 m, respectively, for cases $Gr = 5 \times 10^5$, 7.5×10^5 and 10^6. Associated to such phenomenon, the region of strong fluid acceleration along the tube axis also becomes more extended. The region affected by the reversed flow as well as the distortion observed on isotherms become, consequently, more important. Regarding the case $Gr = 10^6$ in particular, it is very interesting to observe, Fig. 6(d), that under the strong adverse buoyancy effect caused by a very high heating rate imposed at the tube wall, $q''_W = 19\,750\ \mathrm{W{\cdot}m^{-2}}$, the flow exhibits its 'annular structure' with high velocity downward flow in the core region and an annular recirculation cell that occupies a major portion of the tube length. In fact, such zone, attached to the wall, has approximately initiated at the axial position

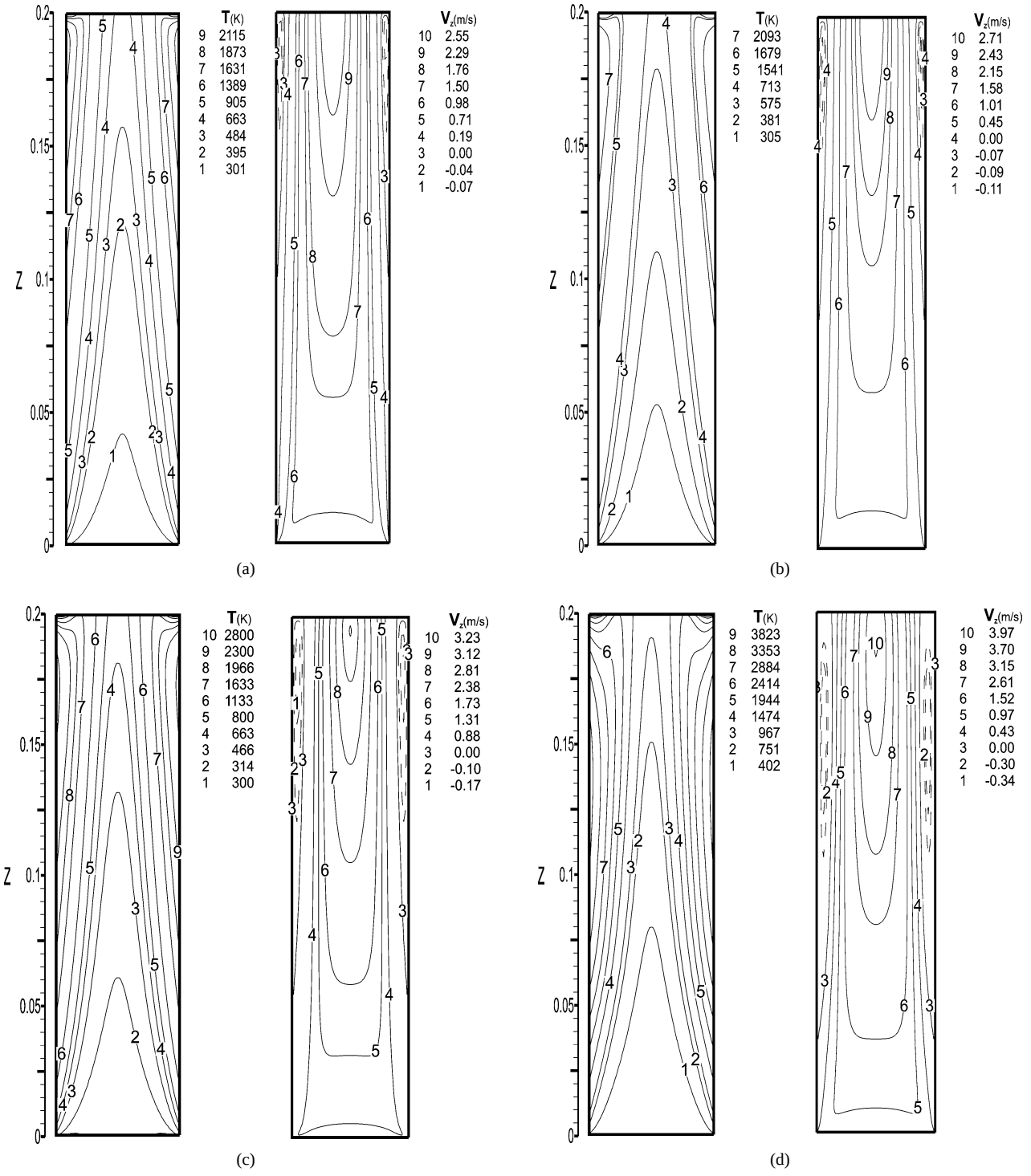

Fig. 6. Transient structure of the flow and thermal field for opposed-buoyancy case (for $Gr = 4.5 \times 10^5$, 5×10^5, 7.5×10^5 and 10^6).

$Z = 40$ mm and is extended up to the exit section; its important thickness is nearly $1/3$ of the tube radius. In the region along the main axis, a rather strong acceleration of the fluid can be remarked. One can also see that the flow field appears to conserve its axisymmetrical character. From the above striking picture of the flow, one can easily expect that the reversed flow region would drastically affect the entire thermal field as shown in Fig. 6(d). It is very interesting to observe that within the recirculation zone, the fluid temperature is considerably higher than that of the surrounding one, in particular in a small area on the tube wall around the center of the recirculation cell where the fluid maximum temperature

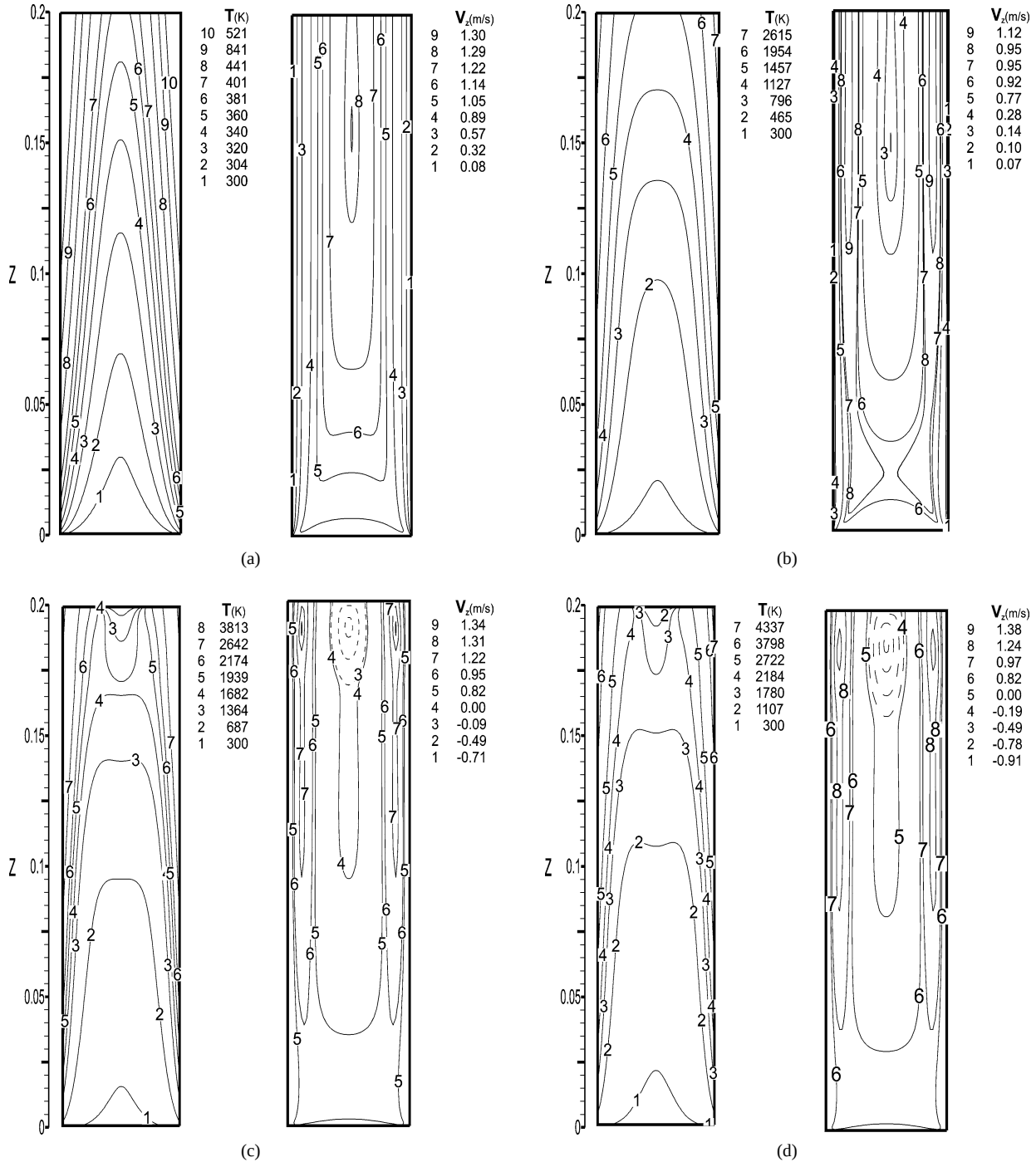

Fig. 7. Transient structure of the flow and thermal field for assisted-buoyancy case (for $Gr = 10^5$, 10^6, 1.5×10^6 and 1.75×10^6).

of order of 3800 K can be remarked. Such rather extreme temperature that may appear somewhat intriguing, can be explained by the fact that fluid that is 'trapped' inside the reversed flow region is continuingly heated by heat input from the wall. Furthermore, heat exchange between this trapped mass of fluid and the surrounding fluid flowing downwards in the core region is mostly accomplished by conduction through their common interface where reduced fluid velocity prevails. As consequence, the 'equilibrium fluid temperature' as high as 3 800 K may then be achieved. With regard to the thermal field near the tube exit section, one can also notice some very interesting behaviour. Thus, due to the reversed flow, fresher fluid at 300 K is coming from the outside environment and flows upstream, which explains the existence of a relatively colder fluid in a narrow region near the exit section.

For the case of assisted-buoyancy flow, results of the flow and the thermal field as obtained for several specific

times corresponding to the following values of the Grashof number, $Gr = 10^5$, 10^6, 1.5×10^6 and 1.75×10^6, are presented in Figs. 7(a)–(d). One can observe, at first, that for the case $Gr = 10^5$ for which only a mild buoyancy effect prevails, the structure of the flow and thermal field appears quite similar to that corresponding to the 'pure-forced convection' case, except for a limited region prior to the tube exit section where we can observe a certain deceleration of fluid in the core region; the velocity ratio V_Z/V_0 is slightly lower than 2. So far, no perceptible effect was noticed on the isotherms structure, Fig. 7(a). With an augmentation in time of q''_W, say for case $Gr = 10^6$ (Fig. 7(b)), as buoyancy effect has considerably increased and resulted in a remarkable acceleration of fluid near the wall and a corresponding deceleration in the core region (see again Fig. 5(a)), the structure of the V_Z-field becomes rather complex. Thus, we can see that the latter now exhibits a narrow annular zone of high fluid velocity gradient near the wall and, essentially, a large central region with low axial velocity. We can also observe that the combination of aiding-buoyancy and boundary layer development has created complex patterns of V_Z contours near the tube inlet section. For case $Gr = 10^6$, there is only small change in the shape of isotherms compared to that of the previous case; with such high level of q''_W, it is obvious that the temperature gradient has considerably increased in the near wall region, while in the core region, isotherms appear to be more flattened. With further increase of q''_W, say for cases $Gr = 1.5 \times 10^6$ (Fig. 7(c)) and 1.75×10^6 (Fig. 7(d)), one can clearly notice the presence of an important reversed flow region that has been developed on the centreline and is attached to the tube exit section through which colder fluid from the outer space is admitted into the domain. Such recirculation zone appears important and it nearly occupies 1/5 of the tube diameter; near the tube exit, its thickness is almost $D/3$ for the case $Gr = 1.75 \times 10^6$. Along the Z-direction, it approximately extends from $Z = 0.09$ m and $Z = 0.08$ m up to the tube exit, respectively, for the cases under consideration. The above intake of fresher fluid has created a localized spot of relatively colder fluid immediately to the exit section that, in turn, has resulted in a higher temperature gradient observed in the near wall region as previously seen in Fig. 5(b). On the other hand, in the entrance region, the structure of the temperature and axial velocity fields appears, essentially, similar to that of the case $Gr = 10^6$ presented earlier.

4. Flow reversal and instability

It has been known that under high wall heat flux condition, especially for the case with opposed buoyancy forces, the flow may exhibit some form of instability [3,4]. Also, as previously stated, the association between the flow reversal phenomenon and the onset of such instabilities, if any, has not yet been clearly established to date [1]. In this study, we have attempted, by performing extended calculations under transient regime in order to investigate such rather interesting issue.

At first, by carefully scrutinizing the structure of both the flow and the thermal field as well as their characteristics while subject to a steadily increasing wall heat flux q''_W during the heating process, it has been observed that, under opposed-buoyancy effect and up to the extreme value of Gr, say $Gr = 10^6$, the flow appears to conserve its axis-symmetrical character. Note that such character has been thoroughly ascertained by establishing the variation of dependent variables, say fluid temperatures and velocity components, along the circumferential direction; also, the fluid tangential velocity component must be zero throughout the domain. The same comment regarding the axis-symmetry also holds for the case of assisted-buoyancy for values of the Grashof number up to 1.75×10^6. It is important to note that the above extreme values of the Grashof number include some 'critical' cases for which no converged solution was possible. These 'critical' cases are, respectively, the ones with $Gr = 7.5 \times 10^5$ and 10^6 for the opposed-buoyancy flow and cases with $Gr = 1.5 \times 10^6$ and 1.75×10^6 for the assisted-buoyancy flow.

In order to investigate the transient behaviors of the flow and thermal field during the heating process and in particular, the flow transition, if any, under critical conditions, i.e., high wall heat fluxes with the presence of the flow reversal, we have thoroughly performed extensive calculations for many Grashof numbers of interest, for both opposed and assisted buoyancy cases. Thus, during the temporal increase of q''_W, see again Fig. 2, immediately after the converged numerical solution has been reached for a specific level of q''_W, say, for example, $q''_W = 1975$ W·m^{-2}, i.e., $Gr = 10^5$, extensive calculations were then pursued for this level of q''_W until the so-called 'asymptotic state' or the 'steady state' of the flow is reached. During all of such calculations, the flow structure and the thermal field as well as their convergence behaviors and the evolution of residuals have been constantly and carefully scrutinized in order to ascertain the nature of the flow, either stable or unstable. On the other hand, for several cases of interest, in order to assess whether the asymptotic flow solution is unique or not, transient calculations have then been performed, starting from other initial conditions and/or using different values of the heating ramp $\mathrm{d}q''_W/\mathrm{d}\tau$, to obtain numerical solutions that correspond to a same final value of q''_W. From such heavy calculation procedure, the following observations seem to be pertinent with regard to the flow stability/instability in the presence of a reversed flow region.

For the case of opposed-buoyancy and Grashof numbers up to the level $Gr = 5.0 \times 10^5$, i.e., $q''_W = 9.875$ W·m^{-2}, no visible sign of transition or instability have been noticed. Also, we have observed that, although the convergence was slightly slower with the increase of the Grashof number, no problems related to the convergence have been experienced so far; residuals as low as 10^{-8} were achieved for all

converged solutions. Such interesting behaviors indicate that the flow appears to remain stable up to the 'critical' level $Gr = 5.0 \times 10^5$. Also, it has been observed that the asymptotic state of the flow that corresponds to a constant level of a wall heat flux q''_W appears to be unique; such asymptotic structure of the flow as well as that of the thermal field have been shown earlier in Fig. 6(a)–(b). We should note that the above 'critical' value of the Grashof number includes, in fact, the case where the flow reversal has just been initiated (case $Gr = 3 \times 10^5$) and also the ones for which the reversed flow region has been well established but remained relatively 'weak' (cases $Gr = 4.5 \times 10^5$ and 5×10^5). This rather interesting behavior seems to indicate that for the opposed-buoyancy flow, the presence of a 'mild' reversed flow region may be somewhat 'tolerated', that is to say that it does not seem to constitute a sufficient condition that triggers the flow transition or instability. Such result appears to be consistent with experimental observations by Lavine and colleagues [5,6]. They have found, by visualization of the downward flow of water in uniformly heated inclined tubes, that the early transition in opposed-buoyancy flow is related, as suggested by Hanratty and colleagues [3,4], to the flow separation from the tube wall; however, the mere presence of such flow reversal does not necessarily guarantee that the flow would become unstable. As we tried to increase the Grashof number beyond the critical value 5×10^5, say for the level $Gr = 7.5 \times 10^5$ that corresponds to $q''_W = 14\,812$ W·m^{-2}, the calculation process has become extremely slow, difficult and rather tedious. For example, it may take a tremendous number of nearly 100,000 'inner iterations' for a single time step; note that no divergence problem has ever been experienced. Also, although the residuals still remain relatively low, they seem to exhibiting some sort of 'cyclic' variation and continued to change as calculations proceeded. Thus, for the case $Gr = 7.5 \times 10^5$ for example, it is observed that the residual of the mass conservation equation has varied between 10^{-5} and 10^{-3}; unfortunately, it was numerically not possible to establish the clear picture of such variation because of the tremendous amount of calculations that would require for. Similar behavior was also observed for the other conservation equations. In fact, as stated previously, the structures of the flow and the thermal fields as shown in Figs. 6(c), (d) were obtained during the course of such difficult calculations, that is to say these structures are actually not converged solutions. The above difficulties regarding the convergence behaviors as well as the evolution of the residuals have become even more drastic for the extreme case of $Gr = 10^6$, see again Fig. 6(d). For the discussed critical cases $Gr = 7.5 \times 10^5$ and $Gr = 10^6$, we did not know, at the present time, what would be the time-evolution of the flow as well as its final state, if any. However, we believe that the above intriguing numerical behaviors may indicate some foresight of a certain transition of the flow to another (unstable?) state. Unfortunately, due to severe limitations of our computer capabilities, we were unable to ascertain such issue at the present time.

For the assisted-buoyancy cases, results and observations from a similar calculation procedure have revealed that both the flow and thermal field seem to remain stable up to the critical level $Gr = 10^6$ or $q''_W = 19\,750$ W·m^{-2}. For case with Grashof number lower than 10^6, the structures of the flow and thermal field also appear to be unique, as previously shown in Fig. 7(a), (b), and this including cases where fluid velocity profiles develop points of inflexion (see again Fig. 5(a)). Such result indicates that the presence of points of inflexion may not constitute a unique and sufficient condition that conducts to instability. Beyond the critical value $Gr = 10^6$, say for the tested cases $Gr = 1.5 \times 10^6$ and $Gr = 1.75 \times 10^6$, similar behaviors regarding the convergence difficulties, as those discussed previously for the opposed-buoyancy flow, have clearly been experienced. And again, although no numerical divergence has been, so far, occurred during the calculation process, no asymptotic or steady state solutions were possible at the present time due to an extremely slow and rather difficult convergence behaviors. In conjunction with that stated previously regarding such behaviors, we believe that some form of flow transition or instabilities may then be expected for cases with Grahof number higher than 10^6. Finally, it is very interesting to note here that for the assisted-buoyancy flow, the above convergence behaviors and numerical difficulties seem to be observed only for cases where the flow reversal has already established; while for cases with sufficiently high Grashof number but without reversed flow, say for the case $Gr = 10^6$, for example (see again Fig. 7(b)), no such difficulties were encountered so far during our calculation procedure. Such result, which indicates that the presence of a reversed flow region appears to be a key factor that may lead to transition and/or instability for an assisted-buoyancy mixed convection flow, has been found to be consistent with that observed experimentally by Hanratty and colleagues [3].

5. Conclusion

In this work, we have numerically studied the problem of the transient mixed convection laminar flow of air inside a vertical tube under buoyancy effect and high Grashof number condition, based on the Boussinesq's assumptions and by using a full 3D-transient model. The imposed wall heat flux is uniform but increases as linear function of time. For the case of opposed-buoyancy, the existence of the reversed flow that is attached to the wall, has been first observed near the tube exit section at the level $Gr = 3 \times 10^5$. With further increase in time, this reversed flow region increases both in volume and in intensity and it clearly progresses upstream. On the other hand, for the case of assisted-buoyancy, results have shown that the onset of the flow reversal on the centreline near the tube exit may be expected for Grashof numbers around 10^6. For

higher value of Gr, such recirculation zone also becomes more important and is spreading upstream. The presence of the reversed flow region has drastically perturbed the internal flow as well as the thermal field. Results have also shown that the structures of the flow and thermal field appear to remain stable and unique up to the level $Gr = 5.0 \times 10^5$ and $Gr = 10^6$, respectively, for opposed and assisted-buoyancy cases. Beyond these critical values, the convergence becomes extremely slow and rather tedious and difficult, which is believed to be due to a certain form of flow transition.

Acknowledgements

The authors wish to sincerely thank the *Natural Sciences and Engineering Research Council of Canada*, the Faculty of Engineering and the Faculty of the Graduate Studies and Research of the '*Université de Moncton*' for financial support to this project.

References

[1] B. Sunden, G. Comini, Computational Analysis of Convection Heat Transfer, WIT Press, Boston, 2000, Chapter 8.
[2] J.D. Jackson, M.A. Cotton, B.P. Axcell, Study of mixed convection in vertical tubes, Internat. J. Heat Fluid Flow 10 (1) (1989) 2–15.
[3] T.J. Hanratty, E.M. Rosen, R.L. Kabel, Effects of heat transfer on flow field at low Reynolds numbers in vertical tubes, Indust. Engrg. Chem. 50 (5) (1958) 815–820.
[4] G.F. Scheele, T.J. Hanratty, Effect of natural convection on stability of flow in vertical pipe, J. Fluid Mech. 14 (1962) 244–256.
[5] A.S. Lavine, M.Y. Kim, C.N. Shores, Flow reversal in opposing mixed convection flow in inclined pipes, J. Heat Transfer 111 (1989) 114–120.
[6] A.S. Lavine, M.Y. Kim, C.N. Shores, Flow reversals in mixed convection in inclined pipes—stability characteristics, in: Proc. ASME–JSME Thermal Engng. Joint Conf., 1987, pp. 645–652.
[7] M. Wang, T. Tsuji, Y. Nagano, Mixed convection with flow reversal in the thermal entrance region of horizontal and vertical pipes, Internat. J. Heat Mass Transfer 37 (15) (1994) 2305–2319.
[8] H. Nesreddine, N. Galanis, C.T. Nguyen, Effect of axial diffusion on laminar heat transfer with low Peclet numbes in the entrance region of a thin vertical tube, Numer. Heat Transfer A 33 (3) (1998) 247–266.
[9] M. Zghal, N. Galanis, C.T. Nguyen, Developing mixed convection with aiding buoyancy in vertical tubes: a numerical investigation of different flow regimes, Internat. J. Therm. Sci. 40 (2001) 816–824.
[10] A. Behzadmehr, N. Galanis, A. Laneville, Low Reynolds number mixed convection in vertical tubes with uniform wall heat flux, Internat. J. Heat Mass Transfer 46 (25) (2003) 4823–4835.
[11] A. Beaudoin, M. Abgrall, J. Padet, Réponse d'un corps de chauffe soumis à un échelon de température, in: Proc. 5è Journées Internationales de Thermique, vol. 1, 1991, pp. 605–613.
[12] L. Fulcheri, R.A. Attalage, Comportement dynamique des émetteurs de chaleur à circulation fluide. Étude théorique et expérimentale, Rev. Gén. Therm. 374 (1993) 77–91.
[13] T.H. Mai, N. El Wakil, J. Padet, Transient mixed convection in an upward vertical pipe flow: temporal evolution following an inlet temperature step, Internat. Comm. Heat Mass Transfer 21 (5) (1994) 755–764.
[14] T.H. Mai, N. El Wakil, J. Padet, Transfert de chaleur dans un tube vertical avec écoulement de convection mixte à débit variable, Internat. J. Therm. Sci. 38 (1999) 277–283.
[15] C.V. Popa, T.H. Mai, Numerical analysis of laminar mixed convection flow instabilities in a vertical pipe, in: Proc. ICHMT/TRCON-03 International Symposium on Convective Heat and Mass Transfer in Single and Two-Phase Flows, 17–22 August 2003, Cesme, Turkey, in press.
[16] L.S. Yao, Is a fully-developed and non-isothermal flow possible in a vertical pipe?, Internat. J. Heat Mass Transfer 30 (4) (1987) 707–716.
[17] L.S. Yao, Linear stability analysis of opposed convection in a vertical pipe, Internat. J. Heat Mass Transfer 30 (1987) 810–811.
[18] L.S. Yao, B.B. Rogers, The linear stability of mixed convection in vertical annulus, J. Fluid Mech. 201 (1989) 279–298.
[19] Y.-C. Su, J.N. Chung, Linear stability analysis of mixed convection flow in a vertical pipe, J. Fluid Mech. 422 (2000) 141–166.
[20] S.W. Yuan, Foundations of Fluid Mechanics, Prentice-Hall, New York, 1967.
[21] S.V. Patankar, Numerical Heat Transfer and Fluid Flow, Hemisphere, McGraw-Hill, New York, 1980.
[22] Fluent 6 User's Guide, Fluent, 2002.
[23] J. Orfi, Convection mixte laminaire dans un tuyau incliné: Développement simultané et phénomène de bifurcation, Ph.D. Thesis, Université de Sherbrooke, Québec, Canada, 1995.
[24] H.L. Langhaar, Steady flow in the transition length of a straight tube, J. Appl. Mech. (1942) A55–A58.
[25] L. Schiller, Die Entwichklung der laminaren geschwindigkeitsverteilung und ihre bedentung für zahigkeitmessungen, Z. Angev. Mech. 2 (1922) 96–106.
[26] W.D. Campbell, J.C. Slattery, Flow in the entrance of a tube, Trans. ASME J. Basic Engng. (1963) 41–46.
[27] W. Pfenninger, Further laminar flow experiments in a 40-foot long 2-inch diameter tube, Rpt. No. AM-133, Northrop Aircraft, Hawthrone, California, 1951.
[28] L. Prandtl, O.G. Tietjens, Applied Hydro-and-Aeromechanics, McGraw-Hill, New York, 1934, p. 27.
[29] C.T. Nguyen, Convection mixte en régime laminaire dans un tuyau incliné soumis à un flux de chaleur constant à la paroi, Ph.D. Thesis, Universitè de Sherbrooke, Québec, Canada, 1988.